Computational Geosciences (2020) 24:1589–1604
https://doi.org/10.1007/s10596-020-09966-1

ORIGINAL PAPER

Iterative geostatistical seismic inversion incorporating local anisotropies

Pedro Pereira[1] · Inês Calçôa[1] · Leonardo Azevedo[1] · Rúben Nunes[1] · Amílcar Soares[1]

Received: 1 August 2019 / Accepted: 8 April 2020 / Published online: 20 May 2020

Abstract
Geostatistical seismic inversion methods use stochastic sequential simulation as the model generation and perturbation technique. These stochastic simulation methods use a global variogram model to express the expected spatial continuity pattern of the subsurface elastic properties of interest. The conditioning to a single variogram model is not suitable for complex and non-stationary geological environments, resulting in poor inverted models unable to reproduce non-stationary features such as channels, folds, and faults. The proposed method uses a stochastic sequential simulation and co-simulation method able to cope with spatially varying information using local and independent variogram models. The information about the dip, azimuth, and ranges of the local variogram model is inferred directly from the observed data. First, local dip and azimuth structural volumes are computed from seismic attribute analysis. Then, local variogram models are fitted along the directions estimated from the previous step. This information is used as steering data during the inversion, acting as proxy of the true subsurface geological complexities. Application examples in synthetic and real datasets with complex geometries show the impact of using local anisotropy models in both the reproduction of the original seismic data and the reliability of the inverted models. The resulting inverted models show enhanced consistency, where small-to-large scale discontinuities and complex geometries are better reproduced, allowing reducing the spatial uncertainty associated with the subsurface properties. This work represents a step forward in integrating geological consistency into geostatistical seismic inversion, surpassing the limitation of using a single variogram model to reproduce complex geological patterns.

Keywords Local varying anisotropy · Geostatistical seismic inversion · Structural seismic attributes · Local variogram models

1 Introduction

Subsurface numerical models are key decision tools that describe the spatial distribution of petro-elastic properties through the integration of multiple sources of data related to the subsurface geology. These models are commonly a result of the geo-modelling workflow, which includes a seismic inversion step [3, 23].

In seismic inversion, the seismic data is used as observed measurements to predict the spatial distribution of the subsurface elastic and/or rock properties. Solving the seismic inversion problem is not straightforward as it is an ill-posed and a highly non-linear problem [47]. This is due to the intrinsic limitations of the seismic method: measurement errors in acquisition and processing steps, the presence of noise, the limited bandwidth and resolution. In addition to the uncertainty in the data, there is also the uncertainty to the modelling process due to the physical assumptions and approximations of the forwarding model. Hence, any prior information about the model parameters should be explicit and include the uncertainties related to the available constraining data to properly model the solution [47]. In seismic inversion, we aim to predict the spatial distribution of the subsurface petro-elastic properties:

✉ Pedro Pereira
pedromartinspereira@tecnico.ulisboa.pt

Inês Calçôa
ines.calcoa@gmail.com

Leonardo Azevedo
leonardo.azevedo@tecnico.ulisboa.pt

Rúben Nunes
nunesrfm@gmail.com

Amílcar Soares
asoares@tecnico.ulisboa.pt

[1] CERENA/DECivil, Arquitetura e Georrecursos, Instituto Superior Técnico, Universidade de Lisboa, Lisbon, Portugal

$$\boldsymbol{d}_{obs} = F(\boldsymbol{m}) + \boldsymbol{e}, \quad (1)$$

where $\boldsymbol{m}$ is any unknown Earth model parameter to be predicted (e.g., acoustic and/or elastic impedances), $\boldsymbol{d}_{obs}$ corresponds to the observed data, F is the forward operator, linking the model parameters and the data, and $\boldsymbol{e}$ is related to measurement error and approximations to the true wavefield propagation.

Seismic inversion methods are classified into deterministic and stochastic [13]. In statistical-based seismic inversion methods, there are two main groups of techniques: the Bayesian linearized approaches, which require the linearization of the forward model and multivariate Gaussian assumption about the a priori model distribution and the error present in the data. Under these assumptions, we are able to define the posterior distribution analytically [3, 14, 25–27, 31, 40]; and geostatistical seismic inversion, which do not need to assume any parametric distribution for the model [1, 2, 5, 6, 8, 11–13, 18, 20–22, 24, 28, 32, 36, 37, 41, 42, 45]. Iterative geostatistical seismic inversion methods (e.g., [2, 3, 4, 5, 11, 28, 29, 37, 44]) perturb and update the model parameter space with stochastic sequential simulation and co-simulation coupled with a global optimizer. The mismatch between real and synthetic seismic drives the iterative procedure and ensures the convergence from iteration to iteration. The resulting models from these methods allow assessing the spatial uncertainty of the inverse solutions [3].

The stochastic sequential simulation and co-simulation require the inversion grid to be regular (i.e., Cartesian grid) and the spatial continuity pattern to be modelled with a global variogram model describing the behavior of the property of interest in the three dimensions of space. The lack of explicit incorporation of structural and stratigraphic information (e.g., folds, faults, discontinuities, and channels) may compromise an accurate inference of the true spatial continuity patterns of the subsurface rock properties. A common procedure to ensure that the inversion grid follows the local stratigraphy is the definition of parallel top and bottom surfaces for the inversion grid, followed by the flattening the original seismic volume by the reservoirs' top or bottom horizon, depending which of these surfaces represents an important unconformity. This simple approach is a proxy of the true structural geology when the seismic reflectors within the inversion area are parallel (or subparallel) relatively to the reference surface (Fig. 1). In the remaining cases, not all the seismic reflectors are flattened and a single global variogram model is not able to capture the true subsurface geological complexities (Fig. 1). In the presence of complex and non-parallel seismic reflections, incorporating information about local anisotropies would help the inversion procedure to reproduce complex geological features.

The geostatistical modelling with local anisotropies has been a topic of interest in subsurface modelling and characterization. Several works have been developed under this scope: a pixel-based geostatistical algorithm accounting for anisotropy information to reproduce curvilinear features of fluvial reservoir models [50]; a gradient algorithm with local anisotropy kriging for mapping curvilinear structures [46] or the splitting of a two-dimensional simulation domain into series of one-dimensional independent spectral simulations along cells connected by each streamline, assuming the a priori knowledge about the curvilinear directions of meandering streamlines [51]. Moreover, some works were proposed to estimate the field of local varying anisotropy using external sources of information to infer the curvilinear distances based on the shortest-paths and nonlinear-distance approaches [9, 10]. In these particular works, external sources of information are required for parameter inference since curvilinear distances cannot be inferred from existing experimental data. In fact, preferable sources of information for estimating local anisotropies include geological interpretations and soft secondary data (i.e., secondary variables) [35]. This is illustrated in [33], where several methods to extract local orientations from a variety of external data sources are developed. Alternatively, a work proposing the simulation of anisotropic properties (e.g., permeability, rock stiffness, or structural anisotropy) through functional Hilbert space decompositions of the random field and spatially varying tensors with uncertain anisotropy is described in [49]. Other works applying a stochastic simulation algorithm with local anisotropy corrections were proposed: to reproduce the connected channel patterns and characterize the spatial distribution over contaminated sediments of a lagoon [29]; for history matching of a non-stationary deltaic reservoir environment [15]; as a seismic interpolation and regularization technique through the application of geostatistical interpolation using local anisotropies estimated from available seismic data [48].

The work presented herein is focused on the integration of stochastic sequential simulation and co-simulation with local anisotropies [15, 29, 48] as perturbation engine of iterative geostatistical seismic inversion. The information about the subsurface local anisotropies is inferred directly from the observed seismic data by seismic attribute analysis. Local dip and azimuth volumes resulting from seismic attribute analysis are used as steering volumes within the inversion. These steering volumes are converted into local variogram models during the stochastic simulation and co-simulation of the elastic models, acting as proxy of a non-Cartesian grid (e.g., [7, 38, 52]) (i.e., the inversion is performed in the original data spatial domain) and surpassing the need of subparallel seismic reflections. The resulting elastic models are more robust and consistent with the main directions of the structural and stratigraphic subsurface geology. We show the application of the proposed methodology to two-dimensional synthetic and three-dimensional real application examples.

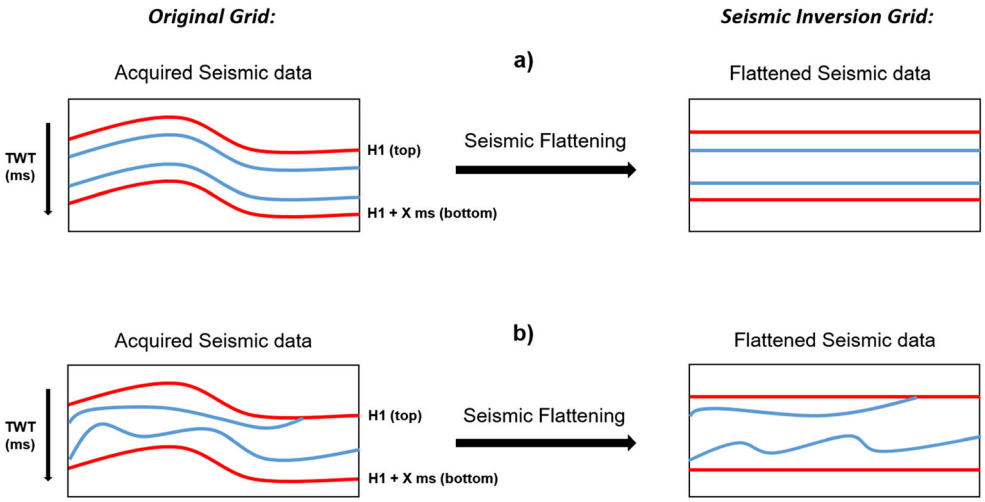

Fig. 1 Schematic representation of the following: (a) flattening of the seismic volume with subparallel reflections; (b) flattening of the seismic volume with non-parallel reflections

2 Methodology

The geostatistical seismic inversion with local anisotropies aims at inverting acoustic impedance from full stack seismic data. The proposed method can be divided in four main stages (Fig. 2): estimation of seismic reflector's orientation (stage 1); automatic variogram modelling (stage 2); model perturbation (stage 3); and stochastic update (stage 4).

2.1 Estimation of seismic reflectors' orientation

In the recent years, the growing of high-quality seismic reflection data led to the proliferation of many seismic attributes [16, 17]. Seismic attribute analysis aims at helping the interpretation of the structural geology, stratigraphy, and rock/pore fluid properties. The estimation of the seismic reflectors' azimuth and dip and the calculation of the attribute along the estimated orientation is a common procedure. This combined approach ensures geological consistency when computing a given seismic attribute [34].

Local structural azimuth and dip are seismic attributes computed following three main steps [30, 39]:

1. estimation of gradient vector ($\nabla x(t_1, t_2, t_3)$), where $x(t_1, t_2, t_3)$ is a seismic sample located in t_1, t_2, t_3;
2. estimation of local gradient covariance matrix $\mathbf{C}(t_1, t_2, t_3)$; and
3. principal component analysis (PCA).

Briefly, in this approach, the local dip and azimuth are first represented by the gradient vector ($\nabla x(t_1, t_2, t_3)$) computed from the original seismic amplitudes [30]. However, the simple calculation of the gradient vectors is too sensitive to noise present in the data and the gradient estimate needs to be smoothed. Due to wraparound effects (i.e., the effects occurring when the angle changes slightly, but its representation changes abruptly, e.g., wrapping from −180 to +180°) the smoothing of the gradient vectors is not trivial [30]. The works introduced in [30, 39] propose to estimate the dip by principal component analysis of the covariance matrix of the gradient vectors. The covariance matrix principal eigenvector is perpendicular to the local reflection dip and azimuth. Thus, the dip and azimuth values are found as a function of the spherical angles of principal eigenvector, $\mathbf{v_1}(t_1, t_2, t_3)$, of the localized covariance matrix, $\mathbf{C}(t_1, t_2, t_3)$; one pair of angle estimates for each voxel. For the complete mathematical description about the computation of these seismic attributes, we suggest to refer to original work in [30].

In this work, the seismic attributes were computed using the available structural attributes (i.e., the local structural azimuth and dip) in Petrel ® software of Schlumberger. A window function of 5 grid cells was applied for the three-directions of space (i.e., *i*-, *j*-, and *k*-directions), corresponding to a Gaussian low-pass filter in order to smooth the azimuth and dip estimates. Different window functions were used during the development of this work, allowing the adjustment between noise sensitivity vs. resolution, and at the same time obtain joint optimum time-frequency resolution [30].

2.2 Automatic variogram modelling

After obtaining the local orientation of seismic events (i.e., local dip and azimuth volumes), local variograms models are estimated at each cell of the inversion grid regarding the three main directions of space. The main direction of the variogram models corresponds to the direction of maximum continuity, given by the local azimuth and dip resulting from the seismic attribute analysis; the minor direction corresponds to the perpendicular horizontal direction for the same sample location; and the normal direction corresponds to the perpendicular direction to the tangent plane (i.e., the plane perpendicular to the direction of maximum discontinuity).

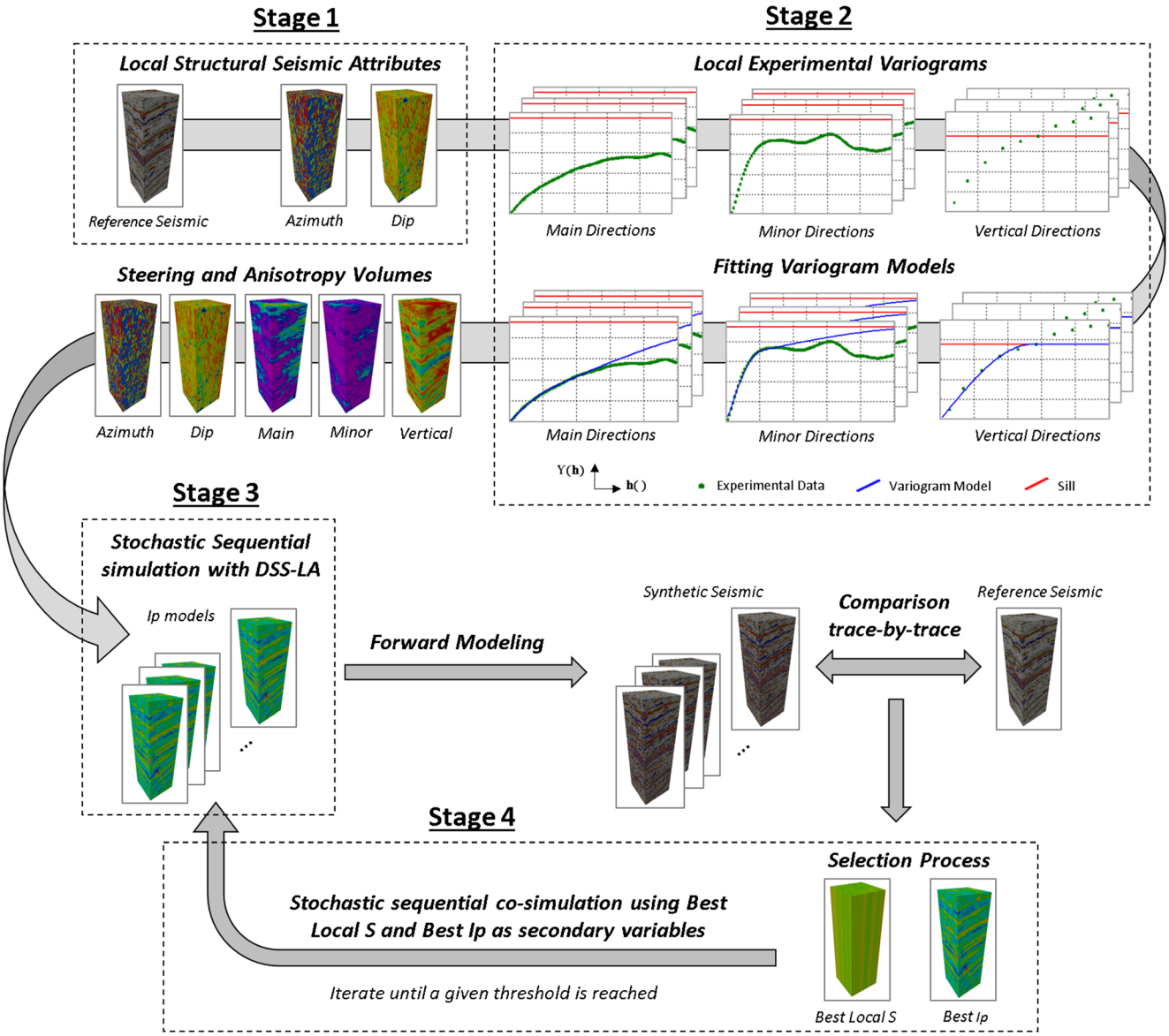

Fig. 2 Proposed methodology main stages

The local variogram modelling is done in two main steps: (1) the estimation of experimental variograms and (2) the automatic fitting of variogram models. These steps are performed sequentially at each grid sample.

The values of local azimuth and dip are integrated in the variogram modelling based on the GSLIB convention for rotation angles, R, associated with the three-dimensional coordinates [19] using the following expression (Eq. 2):

$$R = \begin{bmatrix} \cos(Dip) & -\sin(Dip)*\cos(Dip) & \sin(Az)*\sin(Dip) \\ \sin(Az) & \cos(Az)*\cos(Dip) & -\cos(Az)*\sin(Dip) \\ 0 & \sin(Dip) & \cos(Dip) \end{bmatrix} \quad (2)$$

Then, for each grid sample, the searching neighborhood (i.e., the tolerance pyramids) was parameterized using a tolerance angle, θ, equal to 20° and a lag step of five grid cells. The maximum distances for the searching neighborhood associated with each main direction were defined as follows:

$$D_M = \frac{\max_k}{2}, \quad (3)$$

$$D_m = \frac{\max_k}{4}, \quad (4)$$

$$D_V = 10, \quad (5)$$

where D_M, D_m, and D_V correspond to the maximum distances of searching neighborhood for main (Eq. 3), minor (Eq. 4), and vertical (Eq. 5) directions, respectively. $\max_k$ corresponds to the number of cells in k-direction of the seismic grid (i.e., the vertical direction along the time/depth direction of the grid).

After the searching neighborhood is defined, the local experimental variograms, $\gamma(\boldsymbol{h})$, associated with a given grid sample and with each main direction are computed using the following expression (Eq. 6):

$$\gamma(\boldsymbol{h}) = \frac{1}{2\,N(\boldsymbol{h})} \sum_{\alpha=1}^{N(\boldsymbol{h})} [Z(x_\alpha) - Z(x_\alpha + \boldsymbol{h})]^2, \tag{6}$$

where $N(\boldsymbol{h})$ is the number of pairs of points for each value of $\boldsymbol{h}$ and $Z(x_\alpha)$ is variable used for spatial continuity estimation (i.e., the seismic amplitudes).

It is important to remark that the parameters selected to build the experimental variograms are user-defined and in this work were kept the same for both application examples shown below. However, the parameters may be tuned differently according to the dimensions of the inversion grid (e.g., if the grid is two-dimensional and if corresponds to a vertical or horizontal section).

The local experimental variogram estimated at each grid cell is automatically fitted with a variogram model. Due to its simplicity in terms of implementation and the large number of points in the experimental variogram, we use a least squares fit with a given variogram model (e.g., spherical, exponential, or Gaussian models). In both application examples shown below, we use spherical variogram models. These models were selected after assessing a reasonable number of locations within the inversion grid. After the fitting procedure, we are able to retrieve information about the ranges in the main, minor, and vertical directions.

Both the estimation of the local dip and azimuth and the automatic variogram modelling are two pre-conditioning steps applied before running the inversion, where the local dip, azimuth, and variogram ranges are stored in the auxiliary volumes to be used during model perturbation and update.

2.3 Model perturbation

Direct sequential simulation with local anisotropy corrections (DSS-LA) [15, 29, 48] is used as the model perturbation technique. Acoustic impedance models (Ip) are generated conditioned to the available well-log data and the local variogram models computed a priori directly from the data. Contrary to stochastic sequential simulation methods that rely on a single global variogram model, DSS-LA is able to model curvilinear, non-stationary structures, as for example meandering channels. With DSS-LA, the variogram model may vary across the reservoir grid as it is defined by local variogram parameters (i.e., dip, azimuth, and range following this orientation), rather than imposing a global variogram model and a single orientation as used in conventional DSS. In this framework, each node of the inversion grid is generated, conditioned to the information provided by the steering volumes with information about local anisotropies. Similarly, to DSS algorithm [43], DSS-LA does not require any transformation of the original simulated variable. This approach allows the simulation of structurally consistent properties using traditional Cartesian reservoir grids where the steering volumes are used as proxy of the real complex geology. Within the seismic inversion context, this is an advantage as we no longer need to flatten the original seismic data.

It is worth to mention that using DSS-LA as the perturbation technique of the model parameter space ensures that the probability distribution functions of acoustic impedance, as inferred from the well-log data, are reproduced on each realization generated during the iterative and convergent process. Furthermore, the local spatial continuity pattern, consistent with the subsurface structural and stratigraphic geology, is also reproduced on each realization. In this work, we show the inversion of seismic reflection data directly for acoustic impedance; however, its extrapolation for the AVA domain, where P and S wave velocities and density can be inferred, is straightforward.

2.4 Stochastic update

The stochastic update of acoustic models is established on a data selection procedure performed at the end of each iteration. For a given iteration, and from the set of models generated during the model perturbation stage, the synthetic traces that ensure the highest similarity ($\boldsymbol{S}$) [5, 37] between reference and synthetic seismic data are selected and stored in auxiliary volumes. These volumes are used as secondary variables in the stochastic sequential co-simulation of a new set of models during the subsequent iteration. The variability of the new ensemble of Ip co-simulated in the subsequent iteration is dependent on $\boldsymbol{S}$. If $\boldsymbol{S}$ is close to one, all models will be similar, while $\boldsymbol{S}$ close to zero allow variability within the ensemble of new models. The iterative process finishes when the global $\boldsymbol{S}$ between the synthetic and reference seismic volumes is above a given threshold.

$\boldsymbol{S}$ is the objective function to be maximized in this inversion method, which is simultaneously sensitive to the waveform and amplitude content of the signal:

$$\boldsymbol{S} = \frac{2 * \sum_{s=1}^{N} (\boldsymbol{x}_s * \boldsymbol{y}_s)}{\sum_{s=1}^{N} (\boldsymbol{x}_s)^2 + \sum_{s=1}^{N} (\boldsymbol{y}_s)^2} \tag{7}$$

where x and y are the real and synthetic seismic traces respectively. S measures the similarity between the synthetic and real seismic traces both in terms of waveform and amplitude content.

The schematic representation for the workflow of proposed methodology is illustrated in Fig. 2 and summarized in Algorithm 1.

Algorithm 1 – Iterative geostatistical seismic inversion with local anisotropies

1. Estimate the orientation of seismic reflectors applying seismic attribute analysis;

n = i = j = 1, where n, i and j the grid cell indexes, iterations and simulations respectively;

While n ≤ N, with N the number of grid samples

2. Estimate local experimental variograms and fit variogram models for the three-dimensional directions;

end

3. Store local anisotropies in auxiliary volumes (steering volumes);

Inputs: well-log data, wavelet, full stack seismic, steering volumes (local azimuths, dips and variogram ranges)

While i ≤ I, with I the number of iterations

While j ≤ S, with S the number of simulations

4. Simulate a set of Ip models with DSS-LA conditioned to well-log data;
5. Generate a set of synthetic seismic volumes;
6. Compare the reference seismic and synthetics in a trace-by-trace basis;

end

7. Select traces with highest local *S* and corresponding Ip traces and store them in auxiliary volumes (best volumes);
8. Return to step 4 using co-DSS and the selected volumes in 7 as secondary variables to simulate the new set of Ip models;

end

Outputs: Set of Ip converged inverted models.

3 Application examples

The methodology proposed in this work was applied to a two-dimensional synthetic and a three-dimensional real dataset. The influence of integrating local anisotropies is contrasted by comparing the inverted models of Ip resulting from the proposed approach with those retrieved by geostatistical seismic inversion with a global variogram model where the model parameter space is perturbed with direct sequential simulation (DSS).

In order to simplify the description of the results, two scenarios are defined for both application examples using Geostatistical Seismic Inversion (GSI): GSI with DSS refers to the results obtained by conditioning the inversion with a global spatial continuity patterns; and GSI with DSS-LA refers to the proposed methodology.

3.1 Synthetic application example

A synthetic dataset was created consisting of a two-dimensional grid with 200 by 1 by 200 cells for *i*-, *j*-, and

k-directions, respectively. The dataset consists on the true vertical section of acoustic impedance section and the corresponding full stack seismic. The Ip model is characterized by the presence of several curvilinear features with lower Ip values over a background facies with high Ip and strong anisotropy (Fig. 3a). From the true Ip section, two wells were extracted close to the boundaries of the model. The well-log data were used as experimental data to condition the generation of models during the simulation process for GSI with DSS and GSI with DSS-LA and to estimate the spatial continuity pattern represented by global variogram of the vertical direction for GSI with DSS. The local dip and azimuths were estimated considering a moving window of 5 by 5 by 5 cells in *i*-, *j*-, and *k*-directions, respectively.

The inversion procedure for both methods was defined with the same parameterization consisting of six iterations and sixteen realizations per iteration. The GSI with DSS ran with the true variogram model of the background facies, oriented with a constant dip of 27°. The range used for the horizontal variogram was twenty grid cells and the vertical variogram was five grid cells, fitted by a spherical variogram model.

On the contrary, the ranges of locally varying variogram models for GSI with DSS-LA run were estimated from the

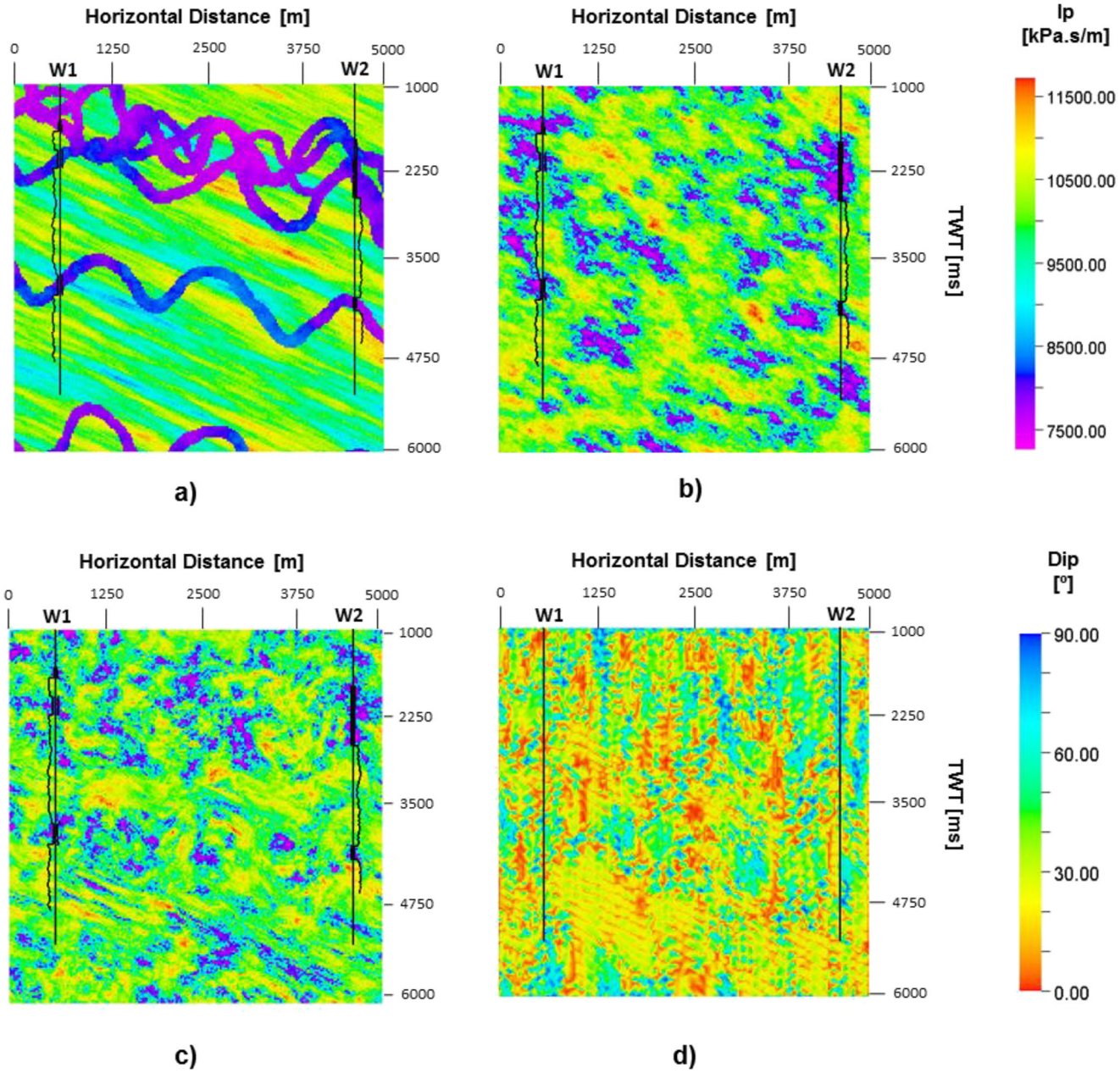

Fig. 3 Vertical sections illustrating (a) the true Ip and the contrasting realizations from first iteration using (b) GSI with DSS, with a constant dip value of 27°, and (c) GSI with DSS-LA conditioned to the (d) dip volume estimated from reference seismic data

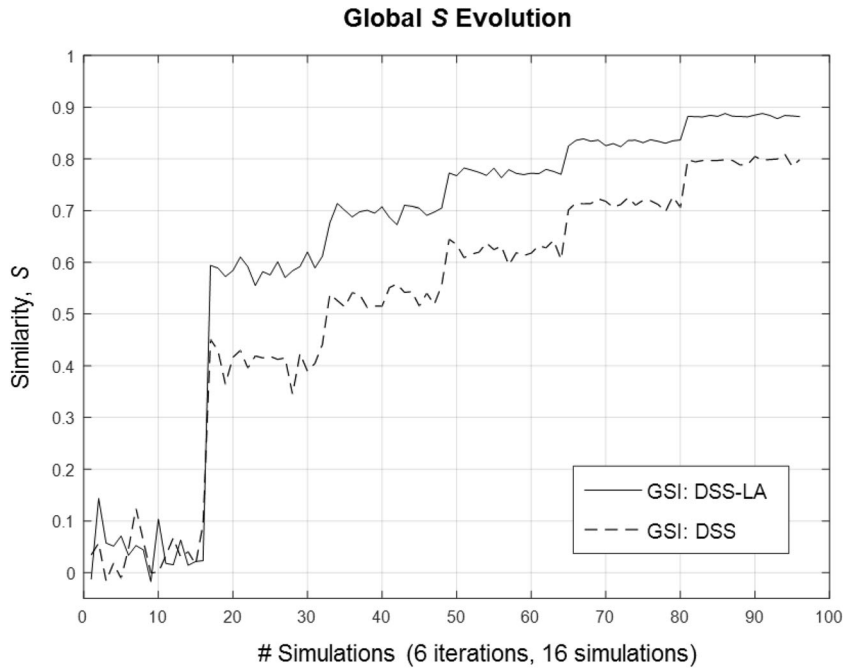

Fig. 4 Comparison between global $\boldsymbol{S}$ evolution of GSI with DSS and GSI with DSS-LA

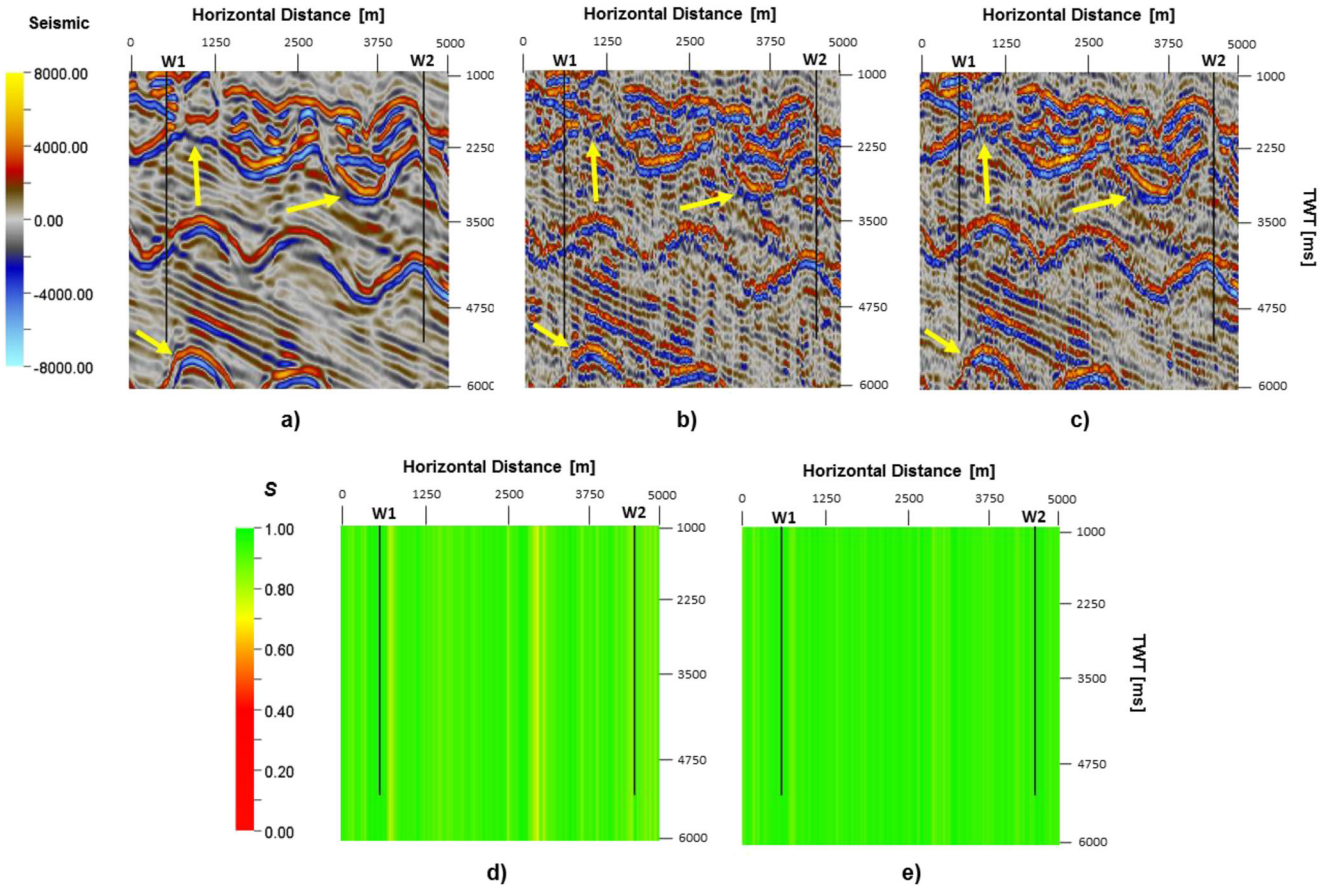

Fig. 5 Vertical time sections of (a) reference seismic data and (b) synthetic seismic computed from Ip best-fit model using GSI with DSS and (c) GSI with DSS-LA; (d) local $\boldsymbol{S}$ using GSI with DSS and (e) GSI with DSS-LA. $\boldsymbol{S}$ is computed from trace-by-trace process between reference seismic and synthetics of Ip models for both methods

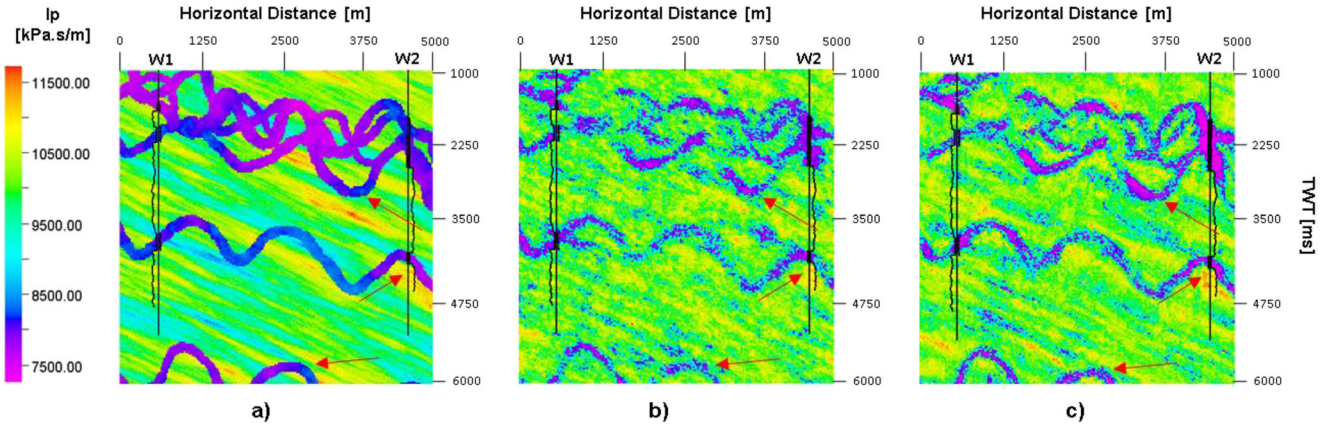

Fig. 6 Vertical sections of (a) true acoustic impedance, (b) Ip best-fit model using GSI with DSS, and (c) GSI with DSS-LA

true seismic amplitudes using the seismic attribute analysis and fitted by spherical variogram models for both directions of the space (Fig. 3d). Two realizations of Ip generated during the first iteration (i.e., simulations not constrained by the seismic data) are shown in Fig. 3 b and c for GSI with DSS and GSI with DSS-LA, respectively. The spatial pattern of the Ip values inferred by the proposed methodology is coherent with the dip section (Fig. 3d).

The evolution of the global $\boldsymbol{S}$ between real and synthetic seismic for both scenarios is shown in Fig. 4. At the end of the inversion process, GSI with DSS-LA achieves a higher global convergence rate of almost 10% when compared with GSI with DSS. The incorporation of information about local anisotropies is critical for the set of Ip models generated during the first iteration. This additional information using DSS-LA allowed to reach about 80% in terms of $\boldsymbol{S}$ after 50 realizations only (i.e., fourth iteration), while the traditional method needed about 80 realizations (i.e., sixth iteration) to reach the same global value. The models generated during the first iteration are already closer to the true subsurface geology, assuming that a reliable anisotropy model is used.

At the end of both inversion processes, the synthetic seismic data from Ip best-fit models for each scenario were computed (Fig. 5 b and c). Although both sections are globally well inverted and similar to the reference seismic (Fig. 5a), there are small-scale features, represented by the yellow arrows (Fig. 5c), which allow to clearly distinguish the differences between the two methods. The highlighted seismic reflectors allow to evaluate the influence of integrating local anisotropies on the heterogeneity associated with the extension and geometry of the curvilinear features. In addition, this impact is corroborated with the sections of trace-by-trace $\boldsymbol{S}$ (Fig. 5 d and e) where the seismic traces in these locations were not so well inverted (Fig. 5d), consequently increasing the uncertainty in the results of GSI with DSS.

The Ip best-fit models obtained at the end of iterative processes are illustrated in Fig. 6. The spatial distribution of higher Ip values of background layers is similar between the inverted solutions from GSI with DSS (Fig. 6b) and GSI with DSS-LA (Fig. 6c), although there are some differences in the absolute values when compared with true Ip section (Fig. 6a). Regarding the geological features of interest, the geometry

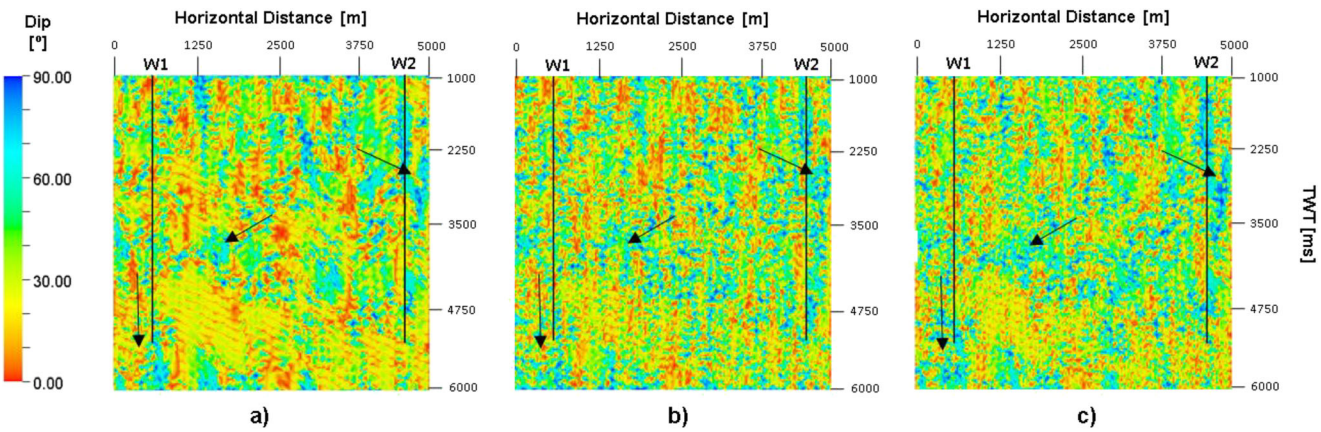

Fig. 7 Vertical time sections of (a) dip estimated from the reflectors of reference seismic data and dip sections estimated from (b) synthetics using GSI with DSS and (c) GSI with DSS-LA

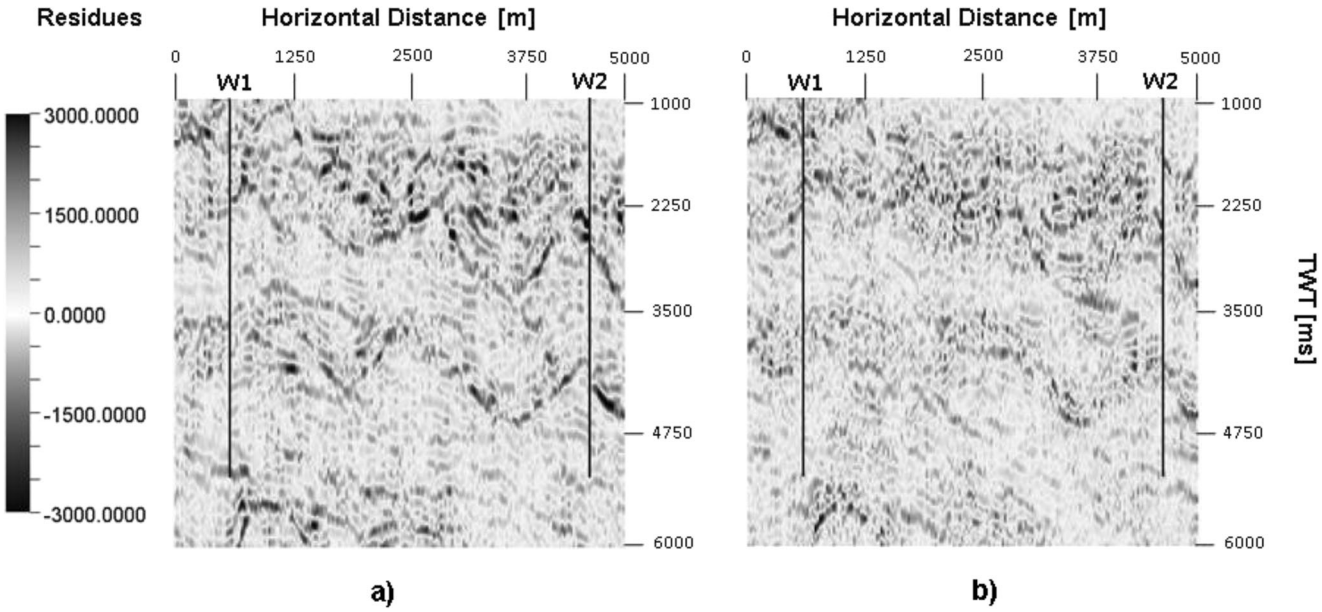

Fig. 8 Vertical time sections of residues between reference seismic data and (a) synthetics using GSI with DSS and (b) GSI with DSS-LA

and connectivity of the curvilinear features are better reproduced with the proposed method as illustrated by the red arrows (Fig. 6).

Figure 7 shows the local dip estimated from seismic attribute analysis over the best-fit synthetic seismic retrieved by both scenarios. In general, the one computed from the proposed method has a better match with the true one, showing higher spatial continuity. The black arrows in Fig. 7c point towards dipping areas where GSI with DSS-LA outperforms the global approach. However, the absolute dip values of horizontal (or subhorizontal) reflectors show similar performances for both methods (Fig. 7b).

The residues between best-fit synthetic and real seismic for both scenarios are shown in Fig. 8. The global approach fails to reproduce the observed seismic amplitudes mainly in areas associated with curvilinear features (i.e., non-stationary features). The difference model for the global inversion (Fig. 8a) has spatially coherent information that has been attenuated by the proposed approach.

3.2 Real application example

We applied the proposed method to a real full stack seismic data to infer the spatial distribution of acoustic impedance models. The inversion grid consists of 100 by 100 by 206 cells in *i*-, *j*-, and *k*-directions, respectively. The seismic was inverted in the original domain (i.e., stratigraphic domain) and no flattening was applied. The spectrum of seismic volume is illustrated in Fig. 9a. The study area consists in a complex turbiditic geological

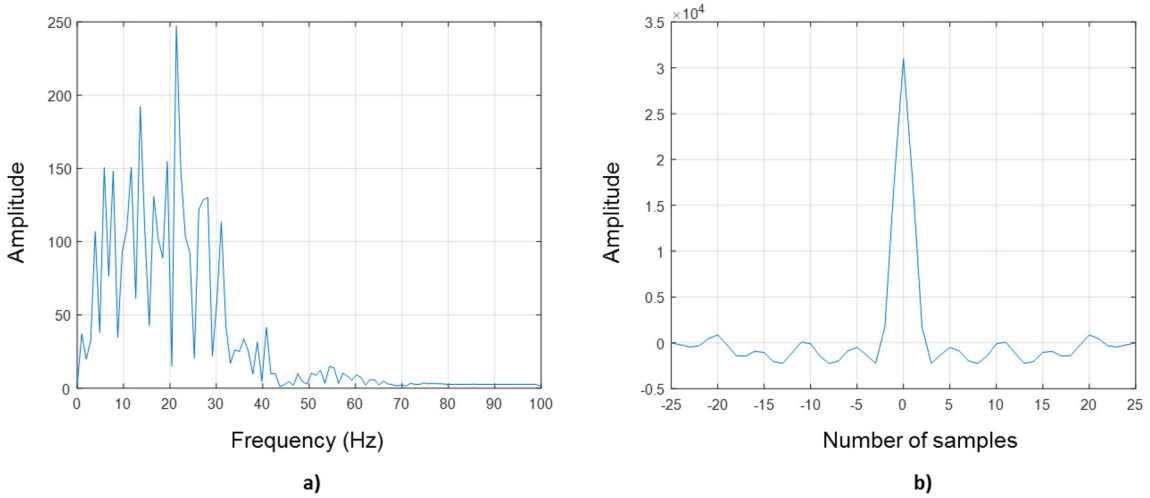

Fig. 9 Seismic spectrum and wavelet used in the inversion process

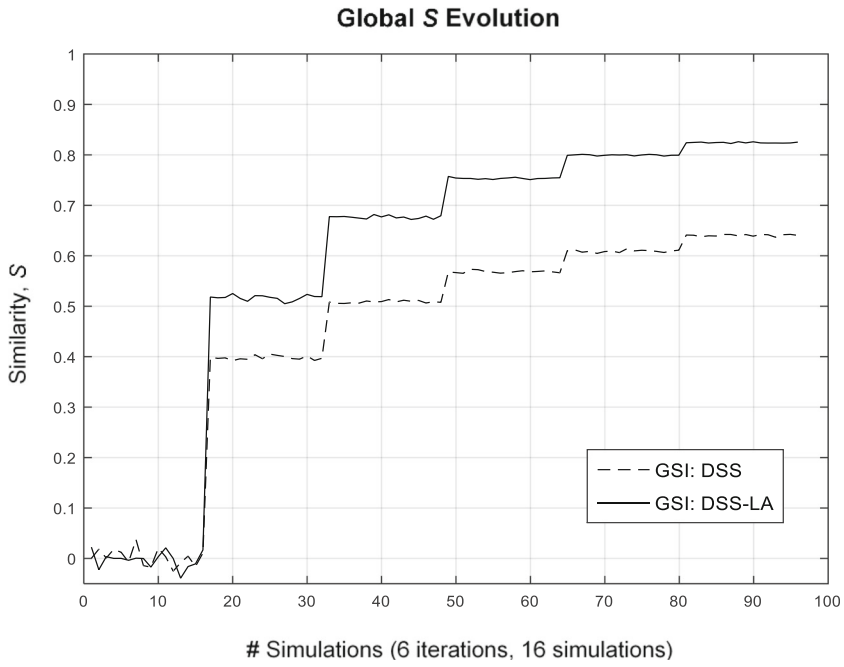

Fig. 10 Comparison between global ***S*** evolution of GSI with DSS and GSI with DSS-LA

environment stratigraphically characterized by the presence of several meandering channels and normal faults throughout the seismic block. This dataset is also completed by Ip well-log data (well W1) and a representative wavelet (Fig. 9b). The local dip and azimuths were estimated considering a moving window of 5 by 5 by 5 cells in *i*-, *j*-, and *k*-directions, respectively.

The local orientation of seismic reflectors was estimated using local structural seismic attributes. These volumes were used to model local variograms for the three main directions of

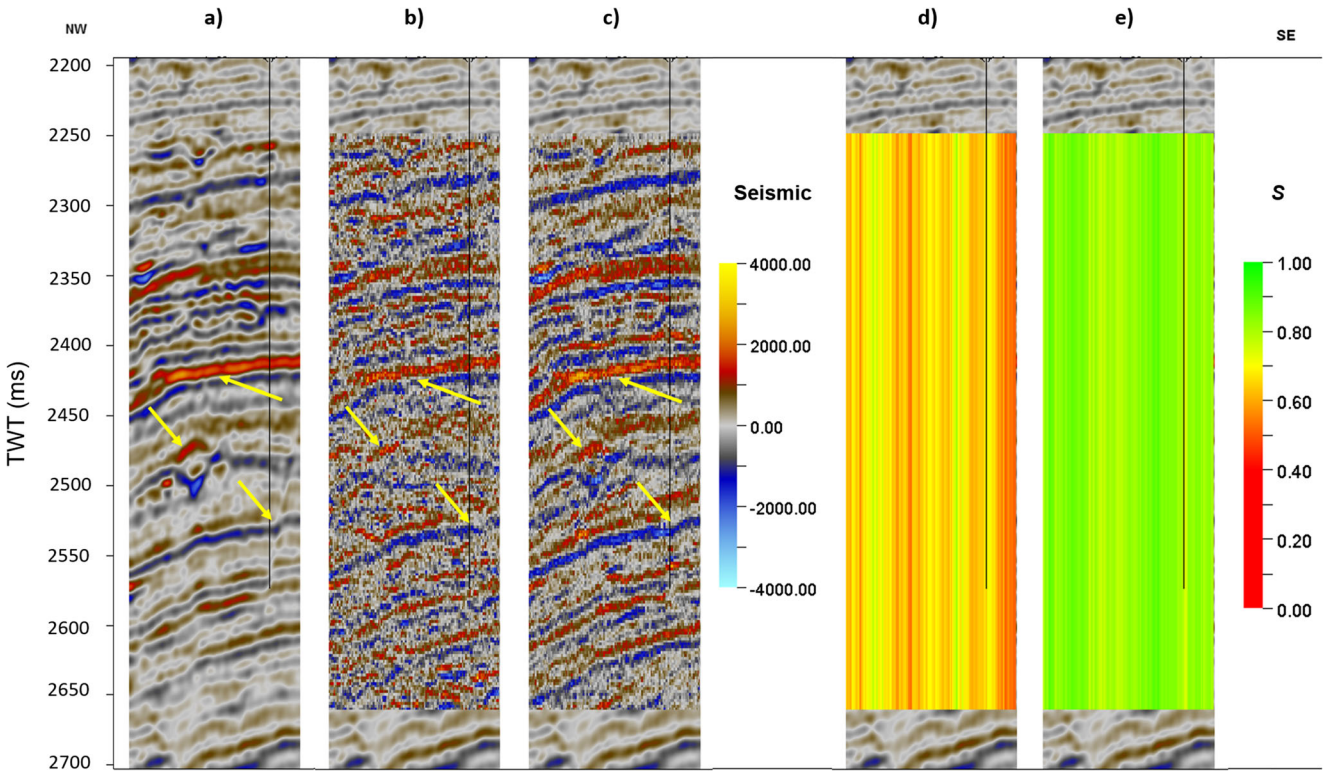

Fig. 11 Vertical time sections of reference seismic data (a) and synthetic seismic computed from Ip best-fit model using GSI with DSS (b) and GSI with DSS-LA (c); and trace-by-trace ***S*** from the best-fit synthetic seismic using GSI with DSS (d) and GSI with DSS-LA (e)

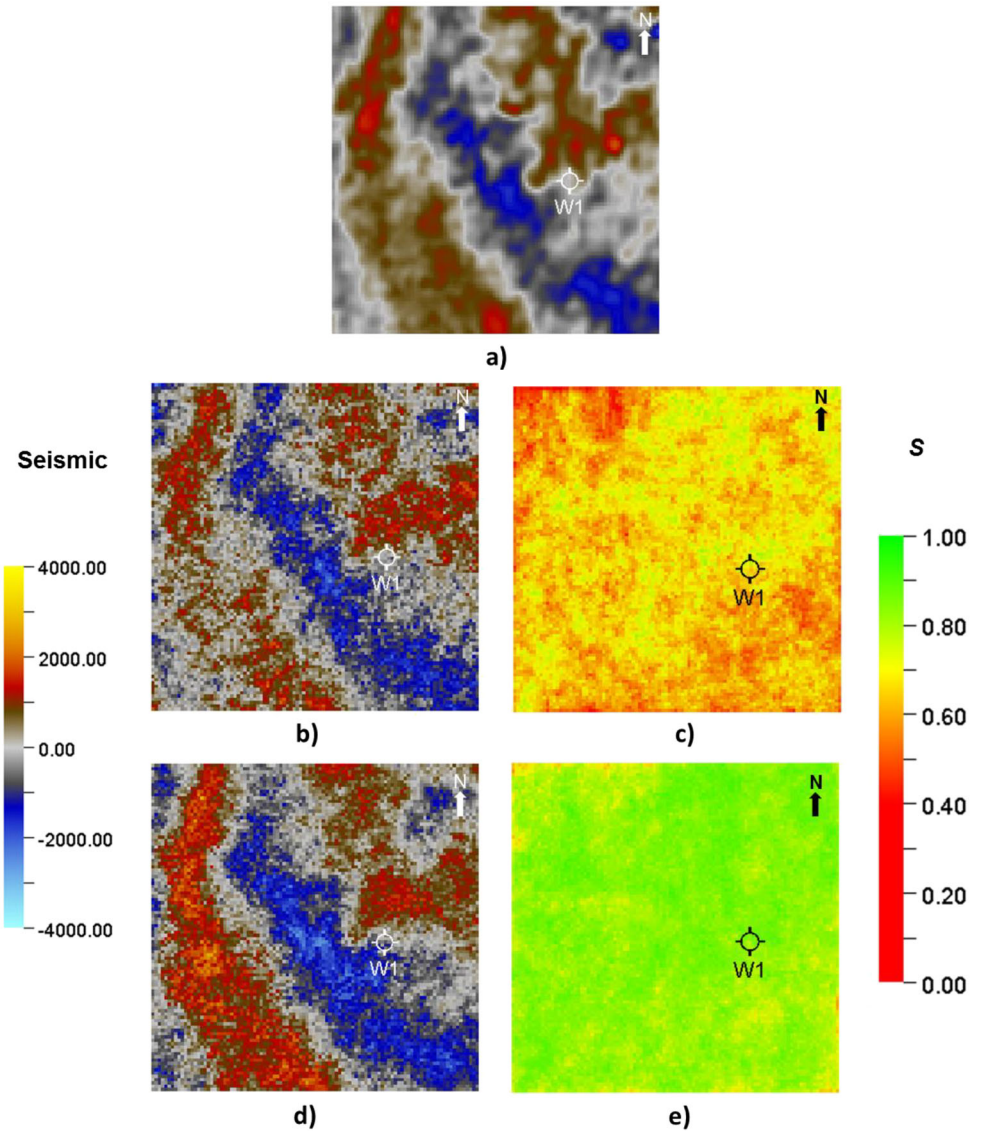

Fig. 12 Horizontal slices ($k = 56$) of reference seismic data (a) and synthetic seismic computed from Ip best-fit model using GSI with DSS (b) and GSI with DSS-LA (d); and trace-by-trace $\boldsymbol{S}$ from the best-fit synthetic seismic using GSI with DSS (d) and GSI with DSS-LA (e)

space for each sample within the inversion grid. For the case of GSI with DSS, the spatial continuity pattern was described by a global omnidirectional spherical variogram model with isotropic horizontal ranges of 15 grid cells and vertical ranges of 5 grid cells.

The seismic inversion runs of GSI with DSS and GSI with DSS-LA were parameterized with six iterations and sixteen realizations for each iteration. The convergence evolution for both methods is shown in Fig. 10. The same behavior as interpreted from the synthetic is observed. Including information about the local anisotropies allows a higher and faster convergence.

The synthetic seismic data computed from the best-fit Ip model are shown using vertical well sections passing through the well (Fig. 11) and horizontal time slices (Fig. 12). The synthetic seismic data resulting from the proposed method (Figs. 11c and 12d) show high similarity with reference seismic (Figs. 11a and 12a), and the seismic reflectors have higher spatial continuity and do better match the true seismic amplitude. This effect is depicted by the trace-by-trace $\boldsymbol{S}$ in Figs. 11d and 12e. In detail, the proposed methodology allows to better image the true stratigraphic and structural features of interest illustrated by the yellow arrows in Fig. 11 a, b, and c.

The best-fit Ip models of both methods are illustrated in Fig. 13. The impact of incorporating local anisotropic information is clearly reflected in the retrieved inverted model by the proposed method. The stratigraphic features of interest appear more spatially consistent (Fig. 13). Particular features of interest, not revealed by the global approach, are the low Ip channels and the presence of normal faults illustrated by the brown arrows (Fig. 13 a and b).

Finally, we compare the local azimuth estimation from the true seismic (Fig. 14a) and estimated from the best-fit synthetic seismic from the traditional (Fig. 14b) and proposed (Fig. 14c) approaches. The inverted seismic applying the

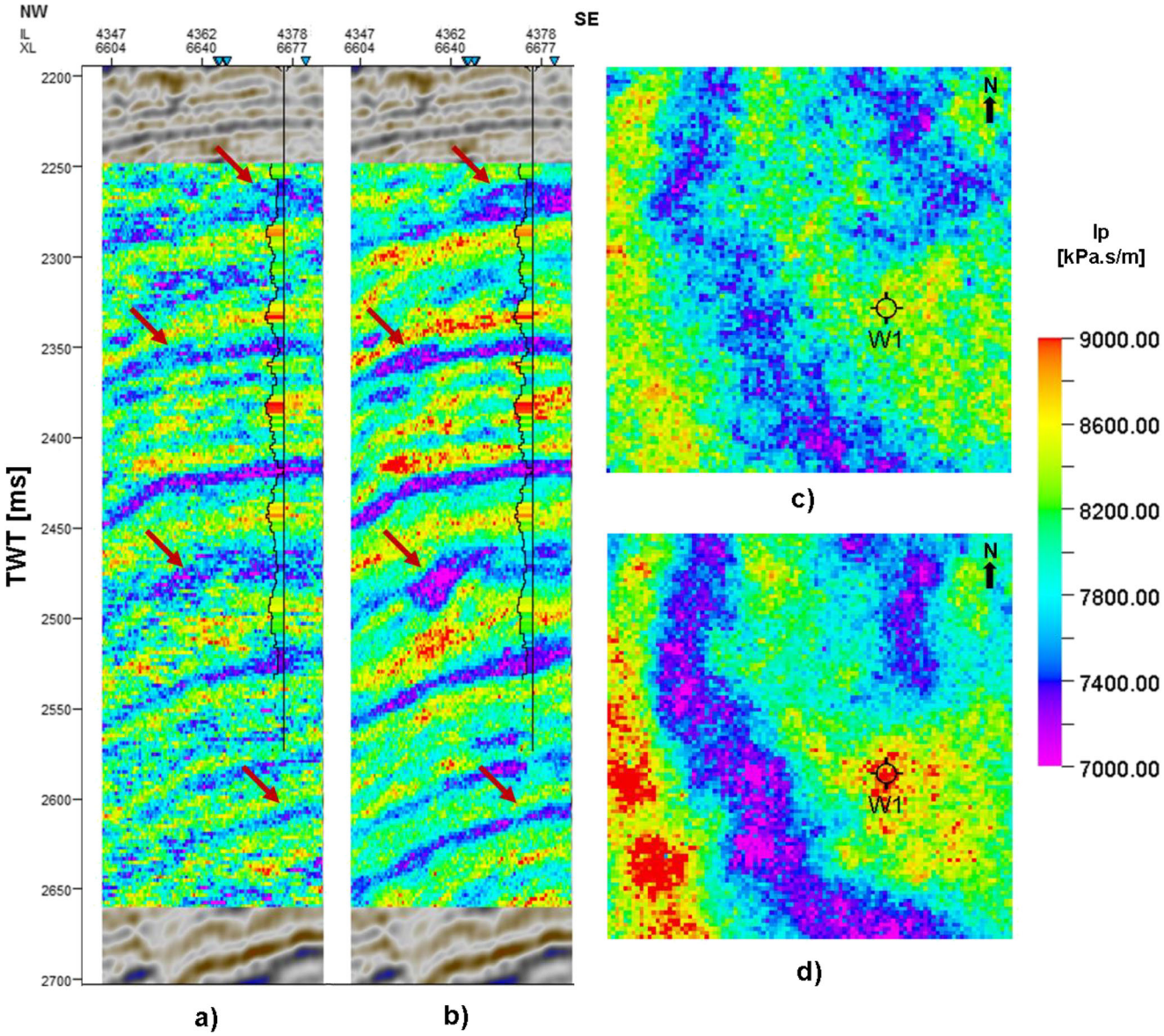

Fig. 13 Vertical time sections of Ip best-fit model using GSI with DSS (a) and GSI with DSS-LA (b); and horizontal slices ($k = 56$) of Ip best-fit model using GSI with DSS (c) and GSI with DSS-LA (d)

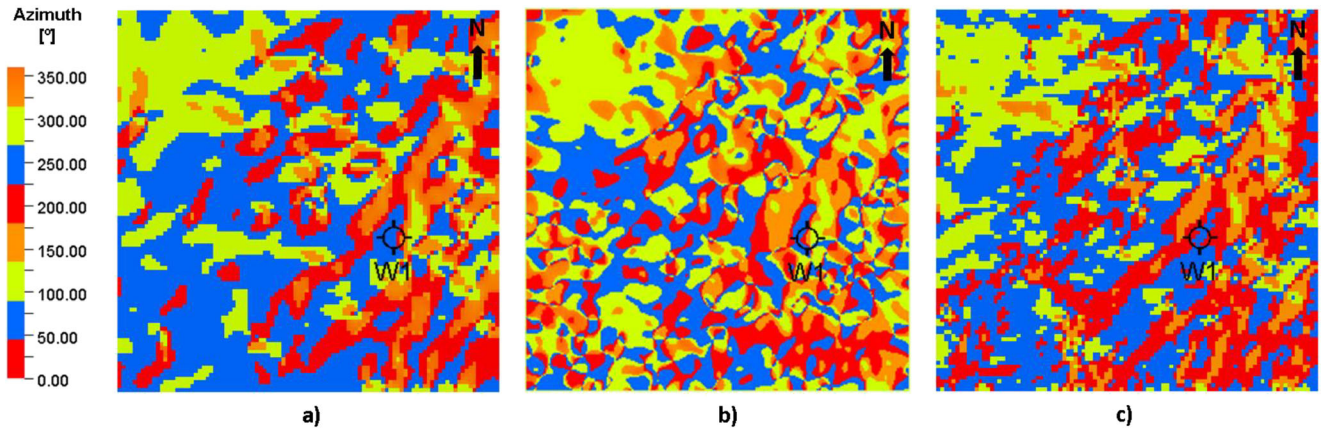

Fig. 14 Horizontal slices ($k = 56$) of azimuth estimated from the reflectors of (a) reference seismic data, from (b) synthetic seismic using GSI with DSS and from (c) synthetic seismic using GSI with DSS-LA

proposed methodology is able to better reproduce the spatial continuity of main features of interest with the correct orientation and dimension.

4 Discussion

We introduce an iterative geostatistical seismic inversion methodology, which allows the incorporation of local varying anisotropies for the simulation of impedance models. The integration of this a priori information to constrain the inversion allows reaching better convergence rates when compared with global approaches (Figs. 4 and 10).

The higher convergence rates are associated with the models generated during the first iteration, which are already closer to the true subsurface geology (Fig. 3). However, the success of the inversion will depend on how reliable the estimation of the local dip and azimuths (i.e., local variogram models) is. The application of state-of-art seismic attribute analysis seems to be a good tool to estimate the local anisotropies. However, as the local anisotropy models are dependent on seismic attributes computed from the observed seismic, we may fail to reproduce sub-resolution features of interest.

Both examples shown here illustrate the benefits of including this type of information during the generation and perturbation of the acoustic models. The Ip models inverted with the proposed method are able to better reproduce channelized features and exhibit higher spatial continuity (Fig. 13). The real case application also shows the ability to better reproduce discontinuities represented by the existing normal faults (Figs. 11 and 13).

Finally, the proposed approach avoids the need of using training images or any other a priori knowledge since the information regarding the spatial continuity pattern of the property of interest is inferred directly from the existing seismic reflection data. In addition, this method alleviates the need of parallel top and base surfaces for the inversion grid and the flattening of the original seismic. This is currently a limitation of global approaches and is used to maximize the horizontalization and spatial continuity of the subsurface properties of interest, allowing the description of its spatial distribution by a single variogram model. As a final remark, it is important to notice that the proposed method requires a higher computational cost, resulting in extra computational hours, when compared with the traditional GSI method. This is due not only to the intrinsic implementation of the stochastic simulation algorithm used during the model perturbation (i.e., methodological step 3) conditioned to local spatial covariance matrices but also due to the estimation of local anisotropy parameters (i.e., methodological steps 1 and 2). Although the estimation of reflector's orientation is relatively fast, the local anisotropy modelling for the three spatial directions requires a higher computational processing and memory cost since the estimation of local experimental variograms and fitting of variogram models is done cell-by-cell.

While the application examples shown here use a fixed variogram model (spherical), this decision may have an impact on the quality and reliability of the inverted models. For this reason, we recommend further analysis on this parameter, which can also be optimized automatically.

5 Conclusions

This work proposes the integration local information about the seismic reflectors' orientation in iterative geostatistical seismic inversion method. This goal is accomplished by extracting information related to local spatial continuity patterns directly from the observed seismic data. A conventional seismic attribute analysis is performed to estimate azimuth and dip volumes. Local variogram models are automatically generated from the local azimuth and dip volumes for each grid cell location within the inversion grid. This information is included as part of the model perturbation stage of iterative geostatistical seismic inversion using stochastic sequential simulation with local varying variogram models.

The proposed method was successfully applied to non-stationary synthetic and real datasets. When comparing against geostatistical seismic inversion techniques based on global variogram models, the inverted models are more robust, showing improved structural and stratigraphic geologic consistency.

While the examples shown here consider acoustic impedance, the extrapolation to other elastic domains (i.e., AVA inversion) is straightforward as long as DSS-LA is used as the model perturbation technique. Furthermore, since the seismic data is the source to generate the steering volumes, the proposed method can be applied to several seismic volumes, when AVA inversion is used.

Acknowledgments The authors acknowledge Partex Oil & Gas for making this dataset available and for the permission to publish it. We also thank Schlumberger and CGG for the donation of the academic licenses of Petrel® and Geoview, respectively. The authors also acknowledge the two anonymous reviewers for their comments during the revision of this paper.

Funding information The authors gratefully acknowledge the support of the CERENA (strategic project FCT UID/ECI/04028/2019).

References

1. Alvarez, P., Bolívar, F., Di Luca, M., Salinas, T.: Multiattribute rotation scheme: a tool for reservoir property prediction from seismic inversion attributes. Interpretation. **3**(4), SAE9–SAE18 (2015)

2. Azevedo, L., Nunes, R., Correia, P., Soares, A., Guerreiro, L., Neto, G.S.: Integration of well data into geostatistical seismic amplitude variation with angle inversion for facies estimation. Geophysics. **80**(6), M113–M128 (2015)
3. Azevedo, L., Soares, A.: Geostatistical Methods for Reservoir Geophysics. Advances in Oil and Gas Exploration & Production. Springer International Publishing (2017)
4. Azevedo, L., Nunes, R., Soares, A., Neto, G.S., Martins, T.S.: Geostatistical seismic amplitude-versus-angle inversion. Geophys. Prospect. **66**(S1), 116–131 (2018)
5. Azevedo, L., Grana, D., Amaro, C.: Geostatistical rock physics AVA inversion. Geophys. J. Int. **216**(3), 1728–1739 (2019). https://doi.org/10.1093/gji/ggy511
6. Bachrach, R.: Joint estimation of porosity and saturation using stochastic rock-physics modeling. Geophysics. **71**(5), O53–O63 (2006). https://doi.org/10.1190/1.2235991
7. Biver, P., Zaytsev, V., Allard, D., Wackernagel, H.: Geostatistics on unstructured grids, theoretical background, and applications. In: Geostatistics Valencia 2016 (2017). https://doi.org/10.1007/978-3-319-46819-8_30
8. Bornard, R., Allo, F., Coléou, T., Freudenreich, Y., Caldwell, D. H., Hamman, J. G.: Petrophysical seismic inversion to determine more accurate and precise reservoir properties: SPE Europec/EAGE Annual Conference, SPE 94144 (2005)
9. Boisvert, J.B., Manchuk, J.G., Deutsch, C.V.: Kriging in the presence of locally varying anisotropy using non-Euclidean distances. Math. Geosci. **41**, 585–601 (2009)
10. Boisvert, J.B., Deutsch, C.V.: Programs for kriging and sequential Gaussian simulation with locally varying anisotropy using non-Euclidean distances. Comput. Geosci. **37**(4), 495–510 (2011)
11. Bortoli, L.J., Alabert, F., Haas, A., Journel, A.G.: Constraining stochastic images to seismic data. Geostatistics Tróia. **1**, 325–337 (1992). https://doi.org/10.1007/978-94-011-1739-5_27
12. Bosch, M.: Lithologic tomography: from plural geophysical data to lithology estimation. J. Geophys. Res. **104**, 749–766 (1999)
13. Bosch, M., Mukerji, T., Gonzalez, E.: Seismic inversion for reservoir properties combining statistical rock physics and geostatistics: a review. Geophysics. **75**, 75A165–75A176 (2010)
14. Buland, A., Omre, H.: Bayesian linearized AVO inversion. Geophysics. **68**, 185–198 (2003). https://doi.org/10.1190/1.1543206
15. Caeiro, M., Demyanov, V., Soares, A.: Optimized history matching with direct sequential image transforming for non-stationary reservoirs. Math. Geosci. **47**, 975–994 (2015). https://doi.org/10.1007/s11004-015-9591-0
16. Chen, Q., Sidney, S.: Seismic attribute technology for reservoir forecasting and monitoring. Lead. Edge. **16**, 445–456 (1997)
17. Chopra, S., Marfurt, K.J.: Seismic attributes – a historical perspective. Geophysics. **70**(5), 3SO–28SO (2005)
18. Coléou, T., Allo, F., Bornard, R., Hamman, J., Caldwell, D.: Petrophysical seismic inversion, SEG, Expanded Abstracts, 1355–1358 (2005)
19. Deutsch, C., Journel. A.G.: GSLIB: Geostatistical Software Library and Users' Guide. Oxford University Press. Volume 136, Issue 1, pp. 83–108 (1998)
20. Doyen, P.M.: Permeability, conductivity, and pore geometry of sandstone. J. Geophys. Res. **93**(B7), 7729–7740 (1988)
21. Doyen, P. M., Guidish, T. M.: Seismic discrimination of lithology: a Monte Carlo approach, in R. E. Sheriff, ed., Reservoir Geophysics: SEG, 243–250 (1992)
22. Doyen, P. M., Den Boer, L. D.: Bayesian sequential Gaussian simulation of lithology with non-linear data: U.S. Patent 5,539,704 (1996)
23. Doyen, P.: Seismic Reservoir Characterization: an Earth Modelling Perspective. Constraints. EAGE (2007)
24. González, E.F., Mukerji, T., Mavko, G.: Seismic inversion combining rock physics and multiple-point geostatistics. Geophysics. **73**(1), R11–R21 (2008)
25. Grana, D., Della Rossa, E.: Probabilistic petrophysical-properties estimation integrating statistical rock physics with seismic inversion. Geophysics. **75**(3), (2010). https://doi.org/10.1190/1.3386676
26. Grana, D., Fjeldstad, T., Omre, H.: Bayesian Gaussian mixture linear inversion for geophysical inverse problems. Math. Geosci. **49**(4), 493–515 (2017)
27. Gunning, J., Glinsky, M.E.: Detection of reservoir quality using Bayesian seismic inversion. Geophysics. **72**(3), R37–R49 (2007)
28. Haas, A., Dubrule, O.: Geostatistical inversion – a sequential method of stochastic reservoir modeling constrained by seismic data. First Break. **12**, 561–569 (1994)
29. Horta, A., Caeiro, M., Nunes, R., Soares, A.: Simulation of continuous variables at meander structures: application to contaminated sediments of a lagoon. In: Atkinson, P., Lloyd, C. (eds.) GeoENV VII – Geostatistics for Environmental Applications, pp. 161–172. Springer, London (2010)
30. Iske, A., Randen, T.: Mathematical methods and modelling in hydrocarbon exploration and production. Mathematics in Industry. (2005). https://doi.org/10.1007/b137702
31. Jullum, M., Kolbjørnsen, O.: A Gaussian based framework for Bayesian inversion of geophysical data to rock properties. Geophysics. **81**(3), R75–R87 (2016)
32. Kemper, M., Gunning, J.: Joint impedance and facies inversion: seismic inversion redefined. First Break. **32**, 89–95 (2014)
33. Lillah, M., Boisvert, J.B.: Inference of locally varying anisotropy fields from diverse data sources. Comput. Geosci. **82**, 170–182 (2015)
34. Marfurt, K.J.: Robust estimates of 3D reflector dip and azimuth. Geophysics. **71**(4), P29–P40 (2006). https://doi.org/10.1190/1.2213049
35. Martin, R., Machuca-Mory, D., Leuangthong, O., Boisvert, J.B.: Non-stationary geostatistical modeling: a case study comparing LVA estimation frameworks. Nat. Resour. Res. **28**, 291–307 (2018). https://doi.org/10.1007/s11053-018-9384-5
36. Mukerji, T., Avseth, P., Mavko, G., Takahashi, I., González, E.F.: Statistical rock physics: combining rock physics, information theory, and geostatistics to reduce uncertainty in seismic reservoir characterization. Lead. Edge. **20**(3), 313–319 (2001)
37. Pereira, P., Nunes, R., Azevedo, L., Soares, A.: The impact of a priori elastic models into iterative geostatistical seismic inversion. J. Appl. Geophys. **170**, 103850 (2019). https://doi.org/10.1016/j.jappgeo.2019.103850
38. Plavnik, A., Sidorov, A.N.: Mapping the properties of geological objects with allowance for anisotropy based on the simulation of the deformation transformation. Mathematical Models and Computer Simulations. **10**(5), 629–638 (2018). https://doi.org/10.1134/S2070048218050095
39. Randen, T., Monsen, E., Signer, C., Abrahamsen, A., Hansen, J. O., Sæter, T., Schlaf, J., Sønneland, L.: Three-dimensional texture attributes for seismic data analysis, S.E.G. Expanded Abstracts, 19 (2000)
40. Rimstad, K., Omre, H.: Impact of rock-physics depth trends and Markov random fields on hierarchical Bayesian lithology/fluid prediction. Geophysics. **75**(4), R93–R108 (2010)
41. Rimstad, K., Avseth, P., Omre, H.: Hierarchical Bayesian lithology/fluid prediction: a North Sea case study. Geophysics. **77**, B69–B85 (2012)
42. Sams, M. S., Atkins, D., Siad, N., Parwito, E., van Riel, P.: Stochastic inversion for high resolution reservoir characterization in the central Sumatra basin: Society of Petroleum Engineers, 57260 (1999)

43. Soares, A.: Direct sequential simulation and cosimulation. Math. Geol. **33**, 911–926 (2001). https://doi.org/10.1023/A:1012246006212
44. Soares, A., Diet, J. D., Guerreiro, L.: Stochastic inversion with a global perturbation method. Petroleum Geostatistics, EAGE, Cascais, Portugal (September 2007): 10–14 (2007)
45. Spikes, K., Mukerji, T., Dvorkin, J., Mavko, G.: Probabilistic seismic inversion based on rock-physics models. Geophysics. **72**(5), R87–R97 (2007). https://doi.org/10.1190/1.2760162
46. Stroet, C., Snepvangers, J.: Mapping curvilinear structures with local anisotropy kriging. Math. Geol. **37**, 635–649 (2005)
47. Tarantola, A.: Inverse problem theory. SIAM (2005)
48. Turco, F., Azevedo, L., Herold, D.: Geostatistical interpolation of non-stationary seismic data. Comput. Geosci. **23**, 665–682 (2019). https://doi.org/10.1007/s10596-019-9812-6
49. Vargas-Guzmán, J.A., Vargas-Murillo, B.: Functional decomposition kriging for embedding stochastic anisotropy. In: Geostatistics Valencia 2016 (2017). https://doi.org/10.1007/978-3-319-46819-8_2
50. Xu, W.: Conditional curvilinear stochastic simulation using pixel-based algorithms. Math. Geol. **28**(7), 937–949 (1996)
51. Yao, T., Calvert, C., Jones, T., Foreman, L., Bishop, G.: Conditioning geological models to local continuity azimuth in spectral simulation. Math. Geol. **39**, 349–354 (2007)
52. Zaytsev, V., Biver, P., Wackernagel, H., Allard, D.: Change-of-support models on irregular grids for geostatistical simulation. Math. Geol. **l48**(4), 353–369 (2016)